Eurasian Chemical Communications

SAMI

FULL PAPER

Adsorptive removal of doxycycline from aqueous solutions by unactivated carbon and acid activated carbon brewery waste grain

Ogunmodede Oluwafemi[a],* ** iD **|Agbogu Emeka[a] |Jonathan Johnson[a] |Osasona Ilesanmi[b] |Oludoro Oluwatosin[a]

[a]*Department of Chemical Sciences, Industrial Chemistry Programme, Afe Babalola University, Ado-Ekiti, Ekiti State, Nigeria*

[b]*Department of Chemistry Bamidele Olumilua University of Education Science and Technology, Ikere-Ekiti, Ekiti State, Nigeria*

This study investigates the adsorptive characteristics of unactivated carbon (UC) and acid activated carbon (AAC) Brewery waste grain BSG for effective DOX removal from aqueous solutions. Batch adsorption experiments were carried out to investigate the sorption behaviour of DOX-adsorbent systems with varying adsorbent doses and initial DOX concentrations. The possibility of mass transfer resistance was examined to improve the diffusion rate, while kinetic aspects were investigated to produce thermodynamic equilibrium for the proposed adsorption process. The degree of ionization of the functional groups of the adsorbate was discovered to have a significant impact on adsorption efficiency. Under optimal reaction conditions, all DOX-adsorbent systems removed more than 90% of the DOX. Before and after adsorption, the shape and functional groups of the adsorbents were investigated. In a kinetic examination, the pseudo-second order kinetic model with normalized standard deviation D_{qt} (percent) 5% and regression coefficient R^2 >0.94 was demonstrated to be more capable of representing kinetic data than the pseudo-first order and elovich kinetic models. For the adsorbate-adsorbent interaction, the applicability of Langmuir and Freundlich isotherms for the proposed adsorption process was examined. DOX had the highest maximum adsorption capacity q_m (0.8576 mgg^{-1} and 0.8216 mgg^{-1}) when using UC and AAC, respectively. Based on the results of thermodynamic studies, the hypothesized process was demonstrated to be exothermic and spontaneous. This study can help better understand industrial waste management as well as an environmentally friendly technology for eliminating DOX from pharmaceutical waste water.

*Corresponding Author:

Ogunmodede Oluwafemi

Email: ogunmodedeo@abuad.edu.ng

Tel.: 08064351797

Introduction

Pharmaceuticals, dyes, heavy metals, pesticide metabolites, and wood processing chemicals, among other things, are increasingly being detected in aquatic ecosystems. Many of these new contaminants, notably pharmaceutically active chemicals, have been detected in treated wastewaters [1] and even in drinking water [2], posing one of the world's biggest environmental issues. The widespread prevalence of these toxins can be attributed to a geometric increase in population, rapid industrialization, a lack of appropriate education on effective contaminant disposal, and a casual attitude among the populace [3]. Heavy and fine chemical effluent from mining, pharmaceutical, and textile industries, for

example, comprises considerable amounts of organic pollutants, toxic chemicals, and a variety of other complex compounds that have deteriorated surface and groundwater quality [4]. One of these contaminants is doxycycline (antibiotic), whose presence in the environment is linked to pharmaceutical effluents. Doxycycline (DOX) is a tetracycline antibiotic that is extensively used in humans and animals to treat infections of the respiratory system, renal failure, and the lungs. It is often favored above other tetracyclines as a supplement in animals' food to speed their growth [5]. The tetracycline antibiotic doxycycline (DOX) is effective against the majority of gram-negative and gram-positive bacteria [6]. It was created in 1967 from tetracycline in order to meet the demand for a drug that could be given on an empty stomach and to reduce the intense 4-times-per-day dosing schedule [7]. Doxycycline is a broad-spectrum tetracycline antibiotic that is used to treat bacterial pneumonia, acne, chlamydia infections, Lyme disease, cholera, typhus, and syphilis, as well as other bacterial and parasitic illnesses [8].
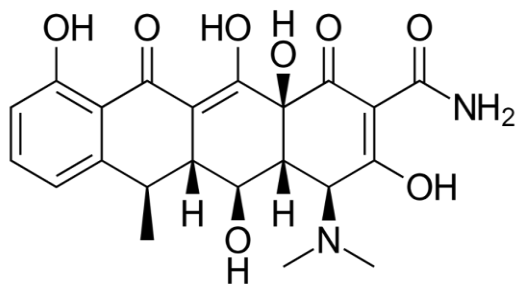
FIGURE 1 Molecular structure of doxycycline ($C_{22}H_{24}N_2O_8$)

Antibiotic use alters microbial ecosystems and exerts selective pressure on susceptible bacteria, resulting in the survival of resistant strains and the development of antimicrobial resistance, rendering existing antibiotics ineffective in the treatment of a wide range of newly emerging infectious diseases [9]. Research reports only a small amount of antibiotics administered to humans and

animals that are digested by the body, with the vast majority excreted unaltered [10]. Doxycycline becomes a contaminant when it is dumped to aquatic bodies as industrial effluent without being effectively treated; as a result, it transforms from a good to a poor product. Because of their solid structure, they are difficult to decompose biologically, putting the environment at risk [11]. Furthermore, because unneeded antibiotics are thrown into municipal waste water, water treatment plants are unable to remove them fully. The water will ultimately reach the surface, seep into the groundwater, and reach drinking water [12]. As a result, the quality of water supplies has degraded, causing harm to humans, plants, and animals. Aside from the long-term effects, antibiotics may cause allergic reactions in some people and change the normal microbial system when they enter the human body via the food chain or drinking water [13]. The negative effects of these toxins on both terrestrial and aquatic life cannot be ignored. Their removal is required to protect the ecosystem from potentially lethal repercussions [14]. As a result, proactive measures have led to the development of various techniques for wastewater treatment, namely photocatalytic, chemical degradation, advanced oxidation, adsorption, coagulation, membrane separation, ion exchange, reverse osmosis, and bioremediation [15,16]. Adsorption is a feasible and cost-effective approach for treating pollutants such as doxycycline and Congo red. It comprises the application of various materials (adsorbents) to the removal of impurities (adsorbates) from aqueous solutions. Clay minerals (montmorillonite, kaolinite, palygorskite, and so on) [17], ozonation [18], electro-flotation, photocatalytic degradation, Fenton degradation, and adsorption are some of the materials that have been utilized to adsorb pollutants. Adsorption is one of the most important research strategies for mitigating DOX pollution in aqueous environments because of its low cost, efficiency, and ability

to be selective or non-selective in nature [19]. Adsorbents such as multiwall carbon nanotubes, activated carbons, zeolites, - cyclodextrin polymer, clay, and metal organic frameworks have been developed to successfully remove antibiotics from aquatic environments [20]. The utilization of natural adsorbents for the adsorption of various pollutants from aqueous medium has sparked considerable attention. The adsorption mechanism of Doxycycline (DOX) was examined at 298, 308, and 318 K using novel acid activated carbon and unactivated carbon from brewery waste grain in this study (BSG). The researchers investigated the effects of pH, ionic strength, contact time, and temperature on DOX adsorption. The mechanisms of DOX adsorption on acid activated carbon and unactivated carbon from brewery waste grain (BSG) have been validated.

Experimental

Materials

The brewery waste grain BSG was supplied by Nigeria Breweries Plc, Ibadan, Oyo State, Nigeria. To remove any remaining moisture, the BSG were thoroughly rinsed in distilled water and sundried for 6 hours before being oven dried at 105 °C. The dried BSG was stored in desiccators to avoid exposure to ambient moisture before being transferred to a well-sealed and airtight container. As a result, BSG is ready for carbonization and activation.

Preparation of doxycycline solution (DOX)

The chemicals in the experiment were all analytical reagent (AR) grade. The doxycycline capsules were supplied by CDA Pharmaceutical and Chemicals. 1g of DOX powder was weighed and diluted in 1 litre of water.

Methods

Carbonization

The BSG was carbonized for 30 minutes at 350 °C in the Afe Babalola University Central Laboratory in Ado-Ekiti, Ekiti State, Nigeria, using a muffle furnace (Vecstar Ltd. England) with limited air supply. The carbonized material was placed in a desiccator and allowed to cool at 25 °C [21].

Chemical activation by phosphoric acid [H_3PO_4]

The chemical activation of carbonized BSG was carried out in accordance with Ekpete and Horsfall's (2011) procedures, applying minor modifications. Samples of carbonized BSG were sieved with a 425 m screen in the Biology Laboratory of Afe Babalola University, Ado-Ekiti, and a carefully weighed amount (25.0 ± 0.01 g) was soaked in a beaker containing 500 cm^3 of 0.3 M Ortho-phosphoric acid (H_3PO_4). The beaker contents were fully mixed before being heated to 60 °C on a magnetic stirrer with a hot plate until a paste formed. The paste was transferred to an evaporating dish and heated in a furnace at 500 °C for 30 minutes. This was allowed to cool to 25 °C overnight. The pH was then stabilized at 7.00 ± 0.2 after being neutralized with KOH and washed with distilled water. This was oven dried to a uniform weight in an airtight 1000 mL reagent container at 105 °C.

Determination of the effect of adsorption contact time

The effect of contact time on sequestering by the two adsorbents was examined by agitating 0.1 g (particle size of 425 m) of unactivated carbon (UC) and Acid Activated Carbon (AAC) with 20 mL of the DOX solution at various contact times ranging from 0 to 90 minutes. After equilibration, the mixture was filtered, and the filtrate was analyzed for residual DOX solution content using a UV-Vis spectrophotometer.

Characterization of the samples

All of the samples were chemically activated carbonized BSG. The adsorbents' Fourier transformed infrared (FTIR) spectra were measured using a Perkin-Elmer spectrophotometer and KBr pellets. A scanning electron microscope (SEM) combined with EDS was used to examine the morphologies and composition of the samples.

Adsorption of doxycycline (DOX)

Chemically activated carbonized BSG was employed in a batch experiment for adsorption studies. The pH variable was determined by weighing 10 mg of each adsorbent (Chemically activated carbonized BSG) into 100 mL beakers containing 15 mL of 0.8 g/L DOX solution with pH ranging from 2 to 10. The ideal pH was determined and applied to further study adsorbent dosage, adsorption duration, and solution temperature.

The absorbance of the remaining DOX in the filtrate was measured with a UV/Vis spectrophotometer model 752 (Gallenkomp, UK) at a wavelength of 362 nm after the adsorbent and DOX solution mixture was filtered under vacuum after agitation. The amount of DOX adsorbed per unit mass of adsorbent was calculated, and the percentage DOX removal (percent R) of each adsorbent was computed using the formula below:

$$\%R = \frac{(C_o - C_f) \times 100}{C_o} \qquad (1)$$

The initial and final concentration of the DOX solutions are C_o and C_f, respectively. The variables of pH and adsorbent dosage; pH and contact time; adsorbent dosage and contact time were statistically analyzed using ANOVA.

Results and discussion

Characterization of adsorbents

Using Fourier Transform Infrared Spectroscopy (FTIR), the spectra of UC, UCA, AAC, and AACA functional groups can be seen in the surface chemistry of the adsorbents (Table 1). Figure 1 shows the characteristic broad peak of O-H stretching vibration of hydroxyl functional groups at 3761.41 cm^{-1} and 3691.66 cm^{-1} [22].

The presence of the O-H stretching bond in both adsorbents verifies BSG's substantial sugar and protein content. The absorption band at 2869.54 cm^{-1} corresponds to the symmetric C-H stretching of the alkane group in cellulose and hemicellulose [23].

Other significant peaks, with bandwidths of 1799.38 cm^{-1} and 1427.00 cm^{-1}, were attributed to aromatic ring C=C and C-H stretching in alkanes and alkyl groups, respectively. The C-O stretching vibration in cellulose, hemicellulose, and lignin is confirmed by absorption peaks at 1233 cm^{-1} and 1100 cm^{-1} [24].

Figure 2 shows the formation of bands 3761.41 cm^{-1} and 3691.66 cm^{-1} in AAC after adsorption, suggesting that doxycycline was adsorbed onto AAC that was not present in the UC. The removal of bands 910.79, 1018, 1633.80, 1826, and 1934 cm^{-1} implies a chemical reaction (chemisorption) on the adsorbent surfaces, whilst the development of several new peaks indicates the possibility of adsorbate-adsorbent interactions [23]. This splitting pattern is typical of a variety of distinct C-O linkages of different phenols, indicating that, as previously noted [25], brewery waste grain may contain cellulose, hemicelluloses, lignin, and a high protein content. The appearance of band 3761.41 cm^{-1} and the deletion of bands 910.79, 1018, 1633.80, 1826, and 1934 cm^{-1} suggested doxycycline (DOX) adsorption on the adsorbents.

TABLE 1 Fourier transform infra-red spectroscopy (FTIR)

| UC		After Adsorption (DOX adsorbed UC)		AAC		After Adsorption (DOX adsorbed AAC)		Remarks
IR PEAK (cm-1)	BOND TYPE	IR PEAK (cm-1)	BOND TYPE	IR PEAK (cm-1)	BOND TYPE	IR PEAK (cm-1)	BOND TYPE	
707.82	Alcohol, O-H out of plane bending	366.38		460.29		707.82	Alcohol, O-H out of plane bending	
872.86		535.11	-	686.69		872.86	-	
1427.63	C-H of methyl bending	707.79	Alcohol, O-H out of plane bending	759.00		1427.63	-	
1798.72		872.86	C-H bending of aromatic ring	910.79	C-H out of plane bending on an aromatic ring	1798.72	-	Disappearance of bands 910.79, 1018, 1633.80, 1826 and 1934 cm3
2517.41		1427.00	C-H bending of methyl	1018.00		2517.41		
2869.54	C-H stretching of methylene	1799.38	C=C ring stretch of aromatic rings	1633.80		2869.54	C-H stretching of methylene	Increase in vibrational band
2926.82	C-H stretching of methylene	2517.24		1826.00		2926.82	C-H stretching of methylene	Disappearance of bands 1826, 1934.33 and 2372.33 cm3
3442.00	OH stretching of Hydroxy group with H-bonding	2870.92	C-H stretching of methylene	1934.33		3442.00	O-H stretching of Hydroxy	
		2929.20	C-H stretching of methylene	2372.33		3691.66	O-H stretching of Hydroxy	
		2969.96	C-H stretching of methyl	2930.12	C-H stretching of methylene	3761.41	Aromatic primary amine N-H stretching	Appearance of band
		3441.00	N-H Heterocyclic amine NH stretching	3690.76	OH stretching of Hydroxy			
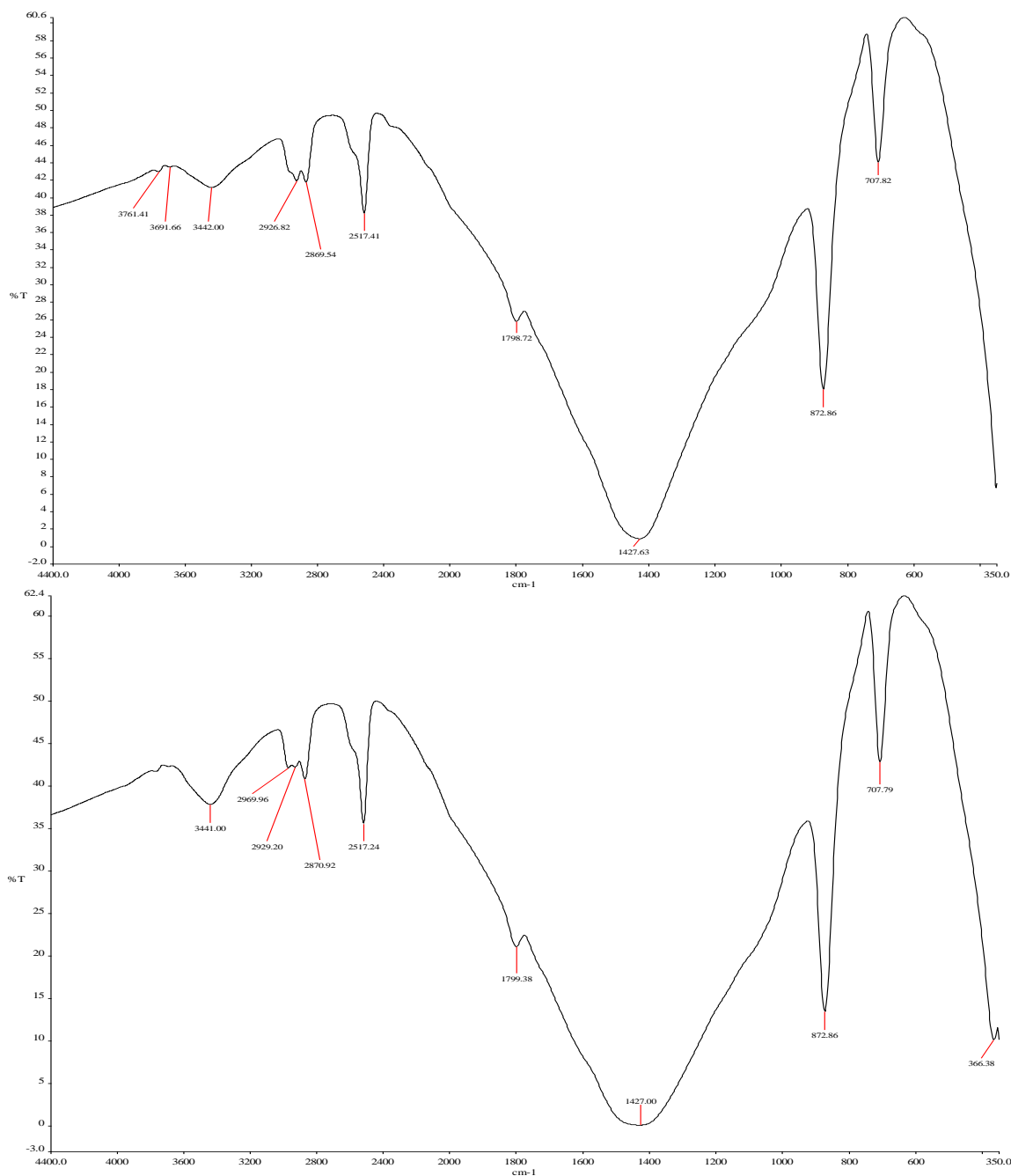
FIGURE 2 FTIR spectra of UC and UCA before and after adsorption of DOX

According to Figure 3, the spectral bands identified in the AACA structure can be attributed to stretching N-H 3761.41 cm^{-1} and asymmetric O-H at 3691.66 cm^{-1} vibrations, C-H stretch indicated by bands in the range of 2926.82 and 2869.54 cm^{-1} [26], and C=O stretching from carboxylic groups and esters indicated by bands in the range of 2926.82 and 2869.54 cm^{-1} [27]. Peaks at around 1600 cm^{-1} and 1700 cm^{-1} indicate the presence of an aromatic ring containing carboxylate groups,

according to Danish *et al.,* [28]. Aromatic group C=C stretching and lignin and C-H vibration from CH2 and CH3 are responsible for the bands detected in the 1450 to 1612 cm^{-1} range [29]. Another band observed in the FTIR spectra of the AACA was at 1035 cm^{-1}, which could be attributed to C-O stretching [26]. The scale expansion in the range of 1400 to 1800 cm^{-1} after DOX adsorption reveals some small alterations in the spectra, as illustrated in Figure 2. At 910.79, 1018,

1633.80, 1826, 1934, 1826, 1934.33, and 2372.33 cm^{-1}, there were minor changes in peak morphology and band displacement. The functional groups attributed to these bands may be implicated in the DOX adsorption process, based on these modifications. DOX adsorption on UC and AAC causes minor vibration frequency changes, which correlate to complexation, chelation, precipitation, and ion-exchange processes [30].
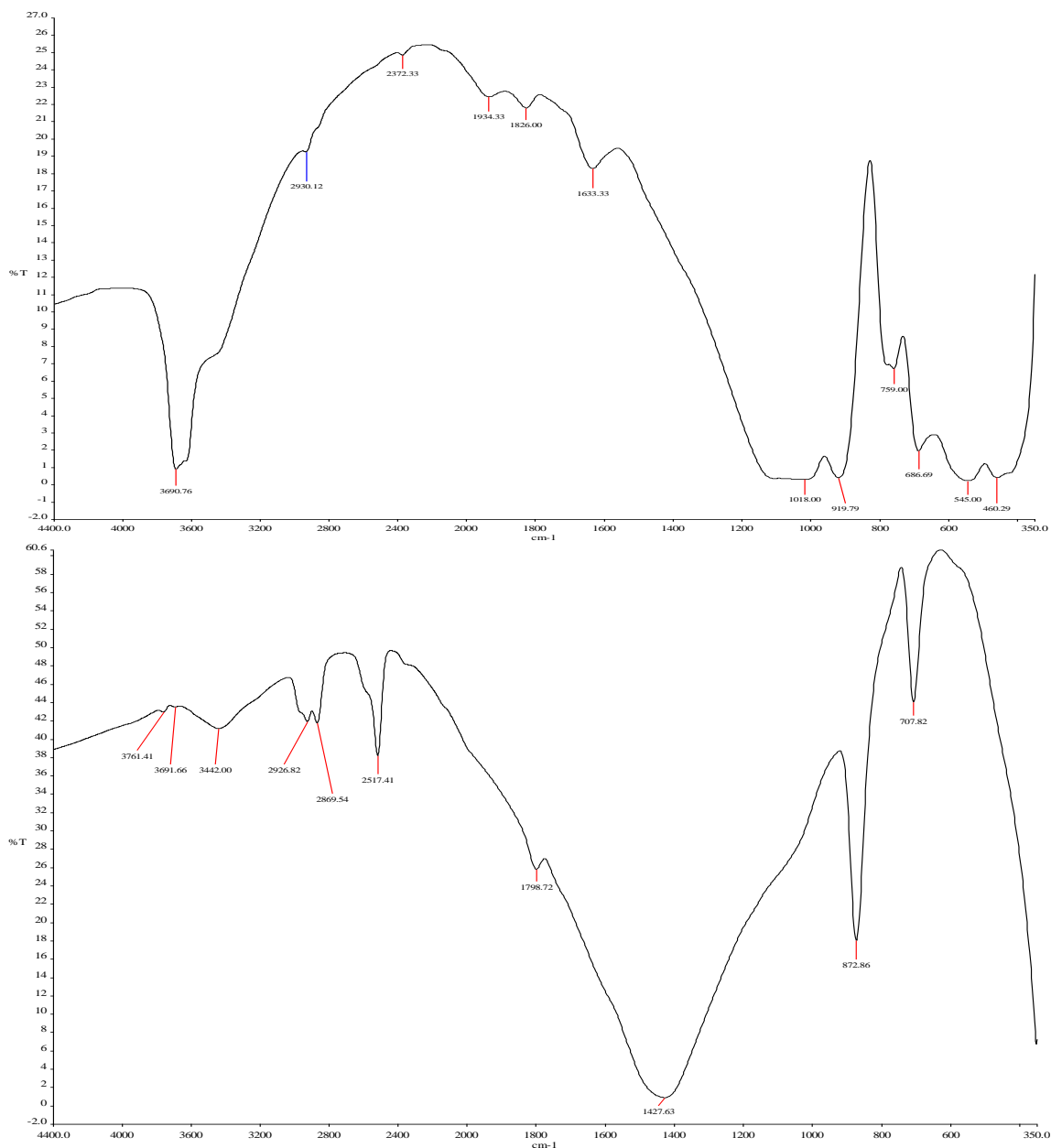

FIGURE 3 FTIR spectra of AAC and AACA before and after adsorption of DOX

Surface morphology

To verify the surface morphology and porosity of the produced adsorbents, a morphological investigation was conducted using high resolution scanning electron spectroscopy (HRSEM). Figure 4 shows the UC, UCA, AAC, and AACA HRSEM images as well as the energy dispersive X-ray spectroscopy (EDX) spectra.
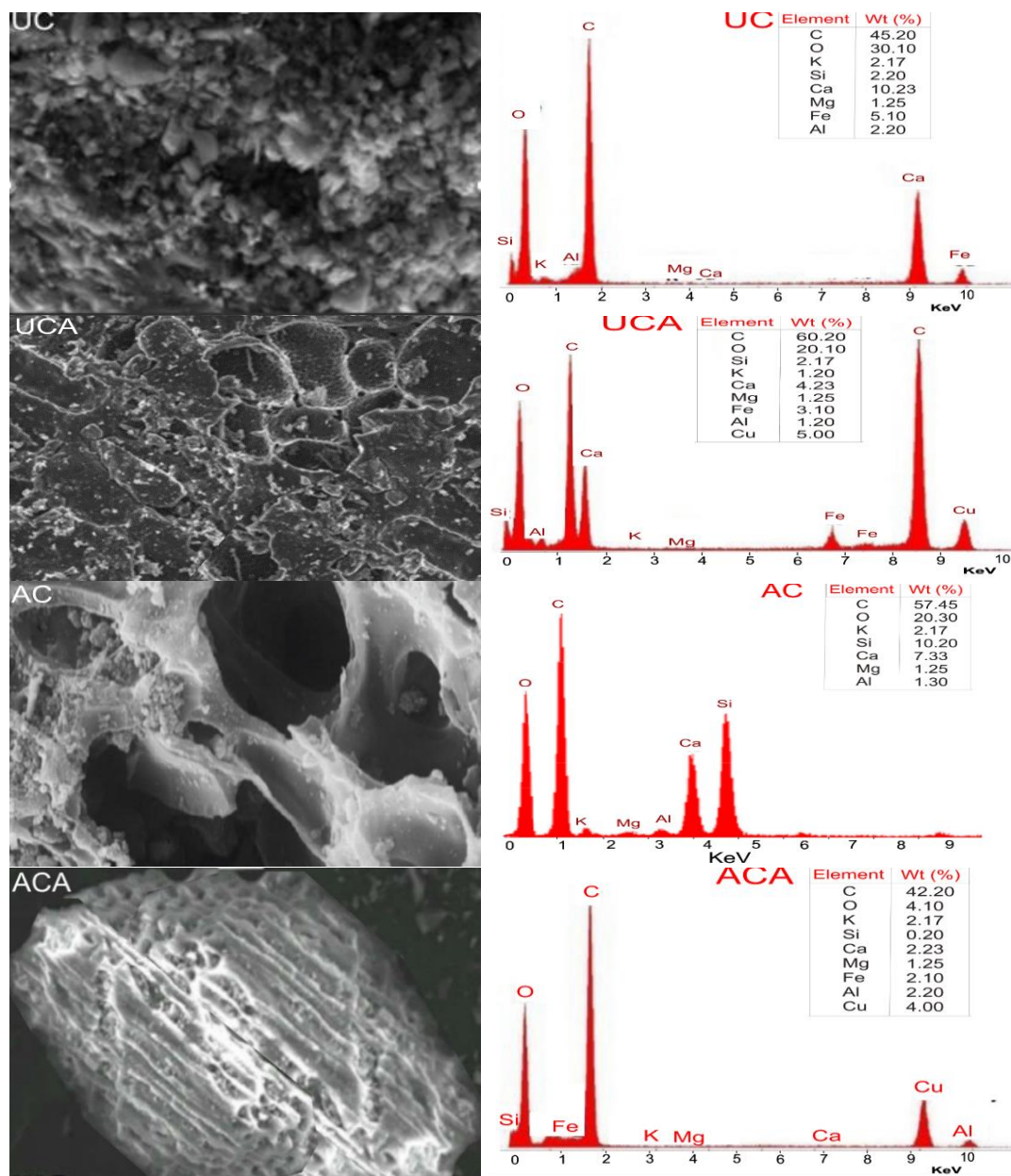
FIGURE 4 HRSEM images with respect to EDX spectra of UC, UCA, AAC and AACA

Micrographs revealed well-developed cavernous porous structures that could aid in the transfer of large amounts of DOX molecules from aqueous solutions to the adsorbent surface. The surface roughness of the DOX-loaded adsorbent changes considerably after adsorption on UC and AAC surfaces. DOX compounds were observed to cover the surface partially. The HRSEM images indicate agglomeration, cluster formation, and a thin layer of DOX on the adsorbents, indicating that the adsorbents are highly efficient at DOX adsorption [31,32]. When the images of all of the samples are compared, it is clear that their morphology and EDX spectra are greatly different. Because the DOX molecule occupied the pores of the adsorbents, the surface of UCA and AACA seemed to be filled. Pores on the adsorbent surface reduce adsorption resistance, allowing DOX solution to enter the adsorbent surface more readily. HRSEM micrographs revealed that the surface morphologies of the adsorbents used in this investigation were all very different. The UCA and AACA pictures reveal less pores on the adsorbents' surfaces,

implying that the DOX solution adhered to the surface, lowering the pore size and surface area of the adsorbents and demonstrating that adsorption occurred and was visible on the surfaces. Figures 4 and 5 show the results of the EDX examination of the adsorbents. Carbon was found in higher amounts than other components in all of the samples, indicating that the adsorbents are carbonaceous. The presence of oxygen after that confirms that the adsorbents used are organic [33]. According to the spectra, the samples comprise C, O, Fe, Ca, K, Al, Cu, and Si. The potassium in the AAC and AACA adsorbents was produced by the KOH manufacturing process on activated carbon. The XRD diffractogram also showed that UC contains the following elements, which predominate due to their percentage abundance C (45.20%), O (30.10%), Ca (10.23%), Mg (1.25%), Fe (5.10%), Al (2.20%), K (2.17%), Si (2.20%): UCA have C (60.20%), O (20.10%), Cu (5.00%), Si (2.17%), Fe (3.10%), K (1.20%), Ca (4.23%), Mg (1.25%), Al (1.20%): AAC have C (57.45%), O (20.30%), K (2.17%), Si (10.20%), Ca (7.33%), Mg (1.25%), Al (1.30%) and AACA have C (42.20%), O (40.10%), Cu (4.00%), K (2.17%), Si (0.20%), Mg (1.25%), Ca (2.23%), Fe (2.10%), Al (2.20). The increase in the percentage concentration of carbon in UC and UCA shows the absorption of DOX molecules, which include an organic component with a carbon skeleton. A drop in the carbon

percentage of AAC and AACA, on the other hand, indicates that chemisorption occurred at the surface of AAC when it came into contact with DOX solution. DOX molecule deposition on the surface of AACA raises the percentage of oxygen content (Figure 4). The potassium concentration of AAC and AACA was due mostly to the KOH used to neutralize the activated carbon and raise the pH to 7.00±0.20 [34]. The presence of silicon in the two adsorbents confirmed that BSG is more than 95% silica, with a high porosity, and a large surface area. Furthermore, the process can be carried out at room temperature without the use of expensive hydrogen. FTIR analysis of the materials revealed the presence of these elements, particularly carbon and oxygen atoms, which are key constituents of sugar and proteins. As a result, BSG contains a high concentration of sugar and protein.

The effect of pH on DOX adsorption sequestration

Solution pH controls the surface properties of adsorbents by changing the degree of ionization of the DOX functional groups and hence plays an important role in the DOX removal process. [22]. As the pH increased, the fraction of DOX eliminated increased progressively until it reached 7, which was the optimum pH for both UC and AAC. As seen in Figure 4, when the pH was raised from 7 to 9, the removal effectiveness of the two adsorbents decreased considerably.
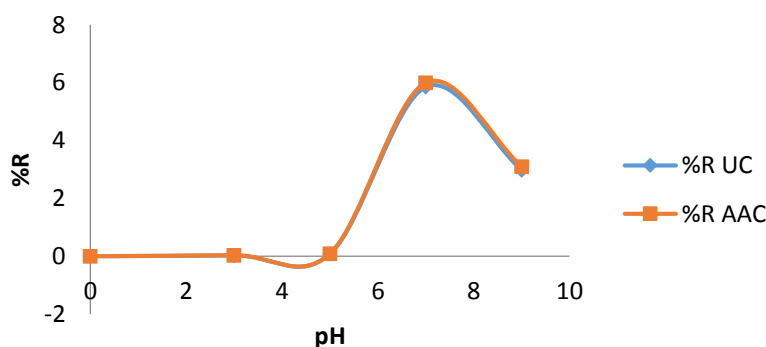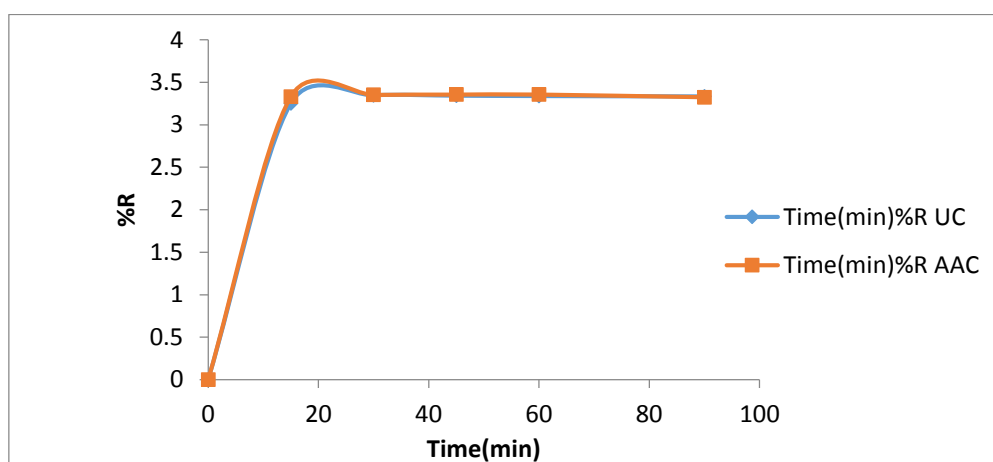

FIGURE 5 Effect of pH on the adsorption of DOX using UC and AAC (Co = 1 g/L, adsorbent dose = 0.1 g and contact time = 60 min)

The pH change appears to have no impact on the removal efficiency. These findings could be explained by the fact that the surfaces of the adsorbents were saturated with the DOX solution H+ at a low pH. As a result, adsorption was poor at pH levels between 3 and 5. However, as the pH rose above 5, the concentration of OH- ions on the surface of the adsorbents increased, which stimulated the adsorption of DOX, albeit only marginally [35].

The influence of contact time on DOX adsorption

Figure 6 shows the influence of contact time on the removal of DOX, indicating that the adsorption rate for both adsorbents was relatively rapid at first. UC and AAC absorbed approximately 3.32 and 3.35 percent of DOX, respectively, within the first 15 minutes of the adsorption procedure. The second step featured sluggish DOX adsorption for UC and AAC ranging from 15 to 90 minutes, with a stable adsorption rate ranging from 5 to 90 minutes of agitation before proceeding at a constant rate. The large number of vacant active sites accessible for DOX adsorption at the start of the procedure, which subsequently decreased until the activated carbon samples were totally saturated, can explain these observations [36].


FIGURE 6 Effect of contact time on the adsorption of DOX using UC and AAC (Co = 1 g/L, adsorbent dose = 0.1 g and contact time = 60 min)

Initial DBT concentration/adsorbent dose ratio influence

Figure 7 shows the results of the sorbent mass dosed effect. The proportion of DOX removed increases as the amount of adsorbent dosed increases, with AAC demonstrating a somewhat higher percentage clearance. As the adsorbent dosage was increased from 0.2 to 1.0 g, the percentage DOX elimination by UC and AAC increased from 2.30-2.63 percent and 2.47-2.70 percent, respectively [37]. Adsorption increases as adsorbent dosage is increased, resulting in the availability of more adsorption sites and a bigger surface area for interaction [38].

The effects of initial concentration are shown in Figure 7. At 298 K, the percent of R by UC and AAC increased from 0.87-3.70 and 0.93-3.80 percent, respectively, while DOX concentration increased from 0.20-1.0 gL^{-1}. This general trend of increasing percentage DOX removal as concentration increases is consistent with previous research [23]. The mass transfer driving force explains the relationship between adsorbent adsorption removal and the concentration of DOX used because when the initial DOX concentration increases, the mass transfer driving force also increase, resulting in greater DOX adsorption [39].
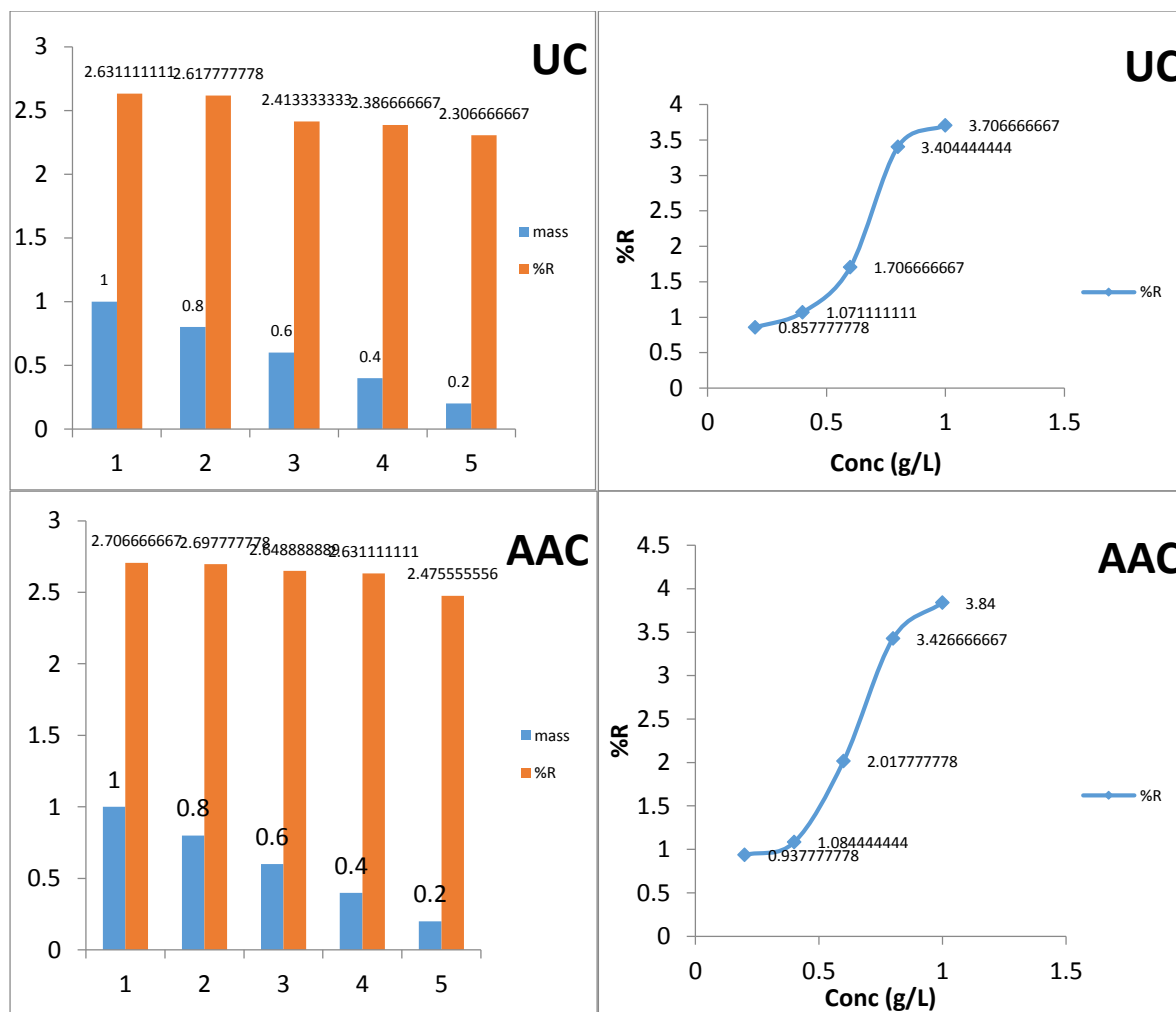
FIGURE 7 Effect of adsorbent dosage and concentration on the adsorption of DOX using UC and AAC

Parameters of the equilibrium adsorption isotherm for DOX adsorption

Equilibrium adsorption isotherms, which are critical in the design of adsorption systems, illustrate the adsorption capacity between the adsorbent (UC and AAC) and various concentrations of DOX at constant temperature. When an adsorbent comes into contact with a DOX solution, the concentration of DOX on the adsorbent's surface rises until a dynamic equilibrium is reached; at this point, the solid and liquid phases have well-defined DOX distributions with no interaction [40].

Langmuir models are the most widely used to depict adsorption data from solutions and isotherms [41].

The expressions for these models are shown below:

The linear form of the Langmuir isotherm is
$$\frac{Ce}{qe} = \frac{1}{KLqm} + \frac{Ce}{qm} \qquad (2)$$

$$Log\ qe = \log Kf + \frac{1}{n}\log Ce \qquad (3)$$

In this study, both models were used to characterize the relationship between the quantity of DOX adsorbed and the compound's equilibrium concentration. The applicability of the isotherm models was determined using the R^2 values of each model. The better the fit, the greater the R^2 value as a measurement of the differences between each individual point and the average fitted curve [42]. The isotherm parameters and related R^2 values for the two DOX-adsorbent (UC and AAC) systems

determined at room temperature are shown in Tables 2 and 3. The correlation coefficients (R^2) demonstrate that the adsorption results best suit the Langmuir adsorption isotherm for UC ($R^2 = 0.94$ at 298K) for the removal of DOX. AAC elimination of DOX at 298K generally followed the Freundlich isotherm model.

TABLE 2 Isotherm parameters for the adsorption of DOX

samples	Langmuir				Freundlich		
	q_m	K_L	R^2	R_L	K_f	n	R^2
UC	0.8576	1.7274	0.94	0.4198	0.46	2.61	0.87
ACC	0.8216	1.9378	0.91	0.3921	0.49	2.91	0.97

NOTE: q_m is in (mgg^{-1}), K_f in $L^{1/n} g^{-1} mg^{-1/n}$, K_L is in Lmg^{-1}

The Langmuir constant is a mathematical constant that describes the relationship between two variables. In terms of a dimensionless metric called separation factor R_L, K_L explains the affinity between the adsorbent and the adsorbate. R_L values are calculated using the formula $R_L = 1/1 + K_L C_o$, where Co is the starting DOX concentration (gl^{-1}) and K_L is the Langmuir constant. The adsorption process is stated to be irreversible if $R_L = 0$, beneficial if $R_L = 1$, and unfavourable if $R_L > 1$. Table 2 shows the R_L values used in this study. At all concentrations considered, the findings suggest that adsorption was favorable (all R_L values are smaller than 1). The Freundlich constant n can be used to forecast the adsorption process' favorability [43]. Table 2 shows that the values of n in this investigation are fewer than one. This is a sign that the process is likely to be successful. The Langmuir and Freundlich isotherm constants can help forecast the success of DOX removal by adsorbents, but they cannot explain chemical or physical features of the process.

Thermodynamics of the adsorption of DOX

TABLE 3 Thermodynamic parameters for the adsorption of DOX

Sample	T (K)	ΔG^0 (J mol^{-1})	ΔH^0 (J mol^{-1})	ΔS^0 (J K^{-1}mol^{-1})
UC	298	-10624.068	-2638.86	26.796
	308	-10891.168		
	318	-11159.988		
AAC	298	-11699.792	-4586.83	23.869
	308	-11938.482		
	318	-12177.172		

To determine the spontaneity of the adsorption process, thermodynamic parameters such as standard entropy change (ΔS^o), standard enthalpy change (ΔH^o), and standard free energy change (ΔG^o) must be determined. Equilibrium investigations at 298, 308, 318 K were used to derive the corresponding values of C_{Ae} and C_e in thermodynamic research [44]. The equilibrium constant Ke can be calculated from C_{Ae} and Ce values using

Ke=C_Ae/Ce   (6)

Where C_{Ae} denotes equilibrium adsorption in gl^{-1} and C_e denotes the DOX equilibrium concentration in gl^{-1}. As shown in the equation 7 below, Vant Hoff's equation is a useful expression that connects ΔH^o and ΔS^o with the equilibrium constant [45]:

ln K$_e$ = -$\Delta H/RT$ + $\Delta S/R$ (7)

Where T is Temperature in Kelvin and R is the gas constant ($Jmol^{-1}K^{-1}$).

The slope and intercept of a plot of ln Ke against 1/T yielded the values of ΔH^o and ΔS^o

whereas the equation below yielded the values of ΔG^{o} at 298, 308, and 318 K.

$$\Delta G^{o} = \Delta H^{o} - T \Delta S^{o} \qquad (8)$$

Table 2 shows the outcomes of these parameters. The exothermic nature of DOX adsorption by the mentioned adsorbents is evidenced by the negative values of ΔH^{o} for DOX adsorbed on UC and AAC. This is a critical value because it means that no additional energy is required for the adsorption process, making it energy independent. Evidently, this adsorption process may be carried out at room temperature, and it becomes more effective as the temperature drops. The negative Gibb's free energy [ΔG^{o}] values for UC and AAC suggest that DOX adsorption by all adsorbents was spontaneous at all temperatures examined. Because the values of ΔG^{o} decreases as the temperature rose, it is possible that the driving power was reduced, resulting in lesser adsorption uptake [46]. The high degree of disorderliness of DOX molecules on the surface of UC and AAC was revealed by the entropy value for DOX sorption on UC and AAC. The positive values of ΔS^{o} found for each adsorbent suggested that throughout the adsorption process, an increase in randomness occurred at the solid-solution interface. This indirectly demonstrates the adsorbent's affinity for DOX molecules [47].

Conclusion

This study highlights the application of novel, low-cost adsorbents for pharmaceutical waste water treatment. The adsorption capability of adsorbents UC and AAC was used to pioneer the removal of antibiotics (DOX) from aqueous solutions. The pH of the solution, the initial DOX concentration, the amount of adsorbent utilized, the agitation period, and the temperature of the solution were all found to be strongly dependent on the technique. The effective adsorption of DOX on both adsorbents was confirmed by characterization

studies. The estimated $q_{e,cal}$ values from the pseudo-second order equation agreed well with the experimental values q_{exp}, showing that the pseudo-second order kinetic model was applicable to all of the adsorption systems investigated. Intra-particle diffusion was demonstrated to influence the DOX absorption process in two stages, with film diffusion taking place first and pore diffusion taking place after agitation. AAC was discovered to be the best adsorbent for DOX adsorption with the highest absorption capacity.

Declaration of competing interest

There are no conflicts of interest.

Orcid:
Ogunmodede Oluwafemi:
https://orcid.org/0000-0001-8571-2979

References

[1] M.I. Vasquez, A. Lambrianides, M. Schneiderc, K. Kümmerer, D. Fatta-Kassinos, *J. Hazard. Mater.*, **2014**, *279*, 169–189. [Crossref], [Google Scholar], [Publisher]

[2] S. Mompelat, B. Le Bot, O. Thomas, *Environ. Int.*, **2009**, *35*, 803-814. [Crossref], [Google Scholar], [Publisher]

[3] B. Li, J. Guo, K. Lv, J. Fan, *Environ. Pollut.,* **2019**, *254*, 113014. [Crossref], [Google Scholar], [Publisher]

[4] Y. Zhao, B. Cao, Z. Lin, X. Su, *Environ. Pollut.*, *254*, 112961. [Crossref], [Google Scholar], [Publisher]

[5] A.C. Kogawa, A. Zoppi, M.A. Quevedo, H.R. Nunes Salgado, M.R. Longhi, *AAPS Pharm Sci*

Tech, **2014**, *15*, 1209-1217. [Crossref], [Google Scholar], [Publisher]

[6] T. Heberer, *Toxicol. Lett.*, **2002**, *131*, 5–17. [Crossref], [Google Scholar], [Publisher]

[7] O.A. Jones, J.N. Lester, N. Voulvoulis, *Trends Biotechnol.*, **2005,** *23*, 163–167. [Crossref], [Google Scholar], [Publisher]

[8] L. Nicole, N. Kennedy, M.C. Clifford, K. Olya, *Environmental Science: Water Research & Technology*, **2017**, *3*. [Crossref], [Google Scholar], [Publisher]

[9] F. Yu, Y. Li, S. Han, J. Ma, *Chemosphere*, **2016**, *153*, 365-385. [Crossref], [Google Scholar], [Publisher]

[10] O.A. Alsager, M.N. Alnajrani, H.A. Abuelizz, I.A. Aldaghmani, *Ecotoxicol. Environ. Saf.*, **2018**, *158*, 114-122. [Crossref], [Google Scholar], [Publisher]

[11] S. Madan, R. Shaw, S. Tiwari, S. Kumar, *Appl. Surf. Sci.*, **2019**, *487*, 907-917. [Crossref], [Google Scholar], [Publisher]

[12] S.J. Olusegun, L.F. de Sousa Lima, N.D.S. Mohallem, *Chem. Eng. J.*, **2018**, *334*, 1719-1728. [Crossref], [Google Scholar], [Publisher]

[13] S.O. Ganiyu, E. Vieira dos Santos, E.C. Tossi de Araújo Costa, C.A. Martínez-Huitle. *Chemosphere*, **2018**, *211*, 998-1006. [Crossref], [Google Scholar], [Publisher]

[14] M.A. Khan, Z.A. ALOthman, M. Naushad, M.R. Khan, M. Luqman, *Desalin. Water Treat.,* **2015**, *53*, 515-523. [Crossref], [Google Scholar], [Publisher]

[16] A.M.S. Solano, S. Garcia-Segura, C.A. Martínez-Huitle, E. Brillas, *Appl. Catal. B Environ,* **2015**, 168, 559-571. [Crossref], [Google Scholar], [Publisher]

[16] Z. Li, N. Potter, J. Rasmussen, J. Weng, G. Lv. *Chemosphere*, **2018**, *202*, 127-135. [Crossref], [Google Scholar], [Publisher]

[17] X. Wang, R. Yin, L. Zeng, M. Zhu, *Environ. Pollut.*, **2019**, *253*, 100-110. [Crossref], [Google Scholar], [Publisher]

[18] Q. Yi, Y. Zhang, Y. Gao, Z. Tian, M. Yang, *Water Research*, **2017,** *110*, 211-217. [Crossref], [Google Scholar], [Publisher]

[19] S. Schwarz, C. Kehrenberg, T.R. Walsh, *Int. J. Antimicrob. Agents,* **2001,** *17*, 431–437. [Crossref], [Google Scholar], [Publisher]

[20] A.L. Batt, I.B. Bruce, D.S. Aga, *Environ. Pollut.*, **2006**, *142*, 295–302. [Crossref], [Google Scholar], [Publisher]

[21] S. Kundu, A.K. Gupta, *Chemical Engineering. Journal,* **2006**, *122*, 93-106. [Crossref], [Google Scholar], [Publisher]

[22] M. Jain, V.K. Garg, K. Kadirvelu, *Journal of Environmental Management*, **2010**, *91*, 949–957. [Crossref], [Google Scholar], [Publisher]

[23] O.A. Ekpete, M. Horsfall, *(Telfairia occidentalis Hook F). Research Journal of Chemical Sciences.,* **2011**, *1*, 2231-606X. [Google Scholar], [Publisher]

[24] S. Banerjee, R.K. Gautam, A. Jaiswal, P.K. Gautam, M.C. Chattopadhyaya, *Desalin. Water Treat.*, **2016**, *57*, 12302–12315. [Crossref], [Google Scholar], [Publisher]

[25] M.A. Ahmad, N. Ahmad, O.S. Bello, *J. Disper. Sci. Technol.*, **2015**, *36*, 670–684. [Crossref], [Google Scholar], [Publisher]

[26] E. Etebu, I. Arikekpar, *Int. J. Appl. Micro. Biotech. Res.*, **2016**, *4*, 90–101. [Crossref], [Google Scholar], [Pdf]

[27] M.J. Dehghan Esmatabadi, A. Bozorgmehr, S.N. Hajjari, A. Sadat Sombolestani, Z.V. Malekshahi, M. Sadeghizadeh, *Cel. Mol. Biol.*, **2017**, *63*, 2, 40-48. [Crossref], [Google Scholar], [Publisher]

[28] S. Mona, A. Kaushik, C.P. Kaushik, *Ecol. Eng.*, **2011,** *37*, 1589–1594. [Crossref], [Google Scholar], [Publisher]

[29] M. Pala, I.C. Kantarli, H.B. Buyukisik, H.B. Yanik, *Bioresour. Technol.*, **2014**, *161*, 255–262. [Crossref], [Google Scholar], [Publisher]

[30] M. Danish, T. Ahmad, R. Hashim, N. Said, M.N. Akhtar, J. Mohamad-Saleh, O. Sulaiman, *Interface Anal.*, **2018,** *11*, 1–13. [Crossref], [Google Scholar], [Publisher]

[31] P. Manara, A. Zabaniotou, C. Vanderghem, A. Richel, *Catal. Today*, **2014**, *223*, 25–34. [Crossref], [Google Scholar], [Publisher]

[32] C. Song, *Catal. Today*, **2003**, *11*, 211–263. [Crossref], [Google Scholar], [Publisher]

[33] A.A. Olajire, J.J. Abidemi, A. Lateef, N.U. Benson, *J. Environ. Chem. Eng.*, **2017**, *5*, 147–159. [Crossref], [Google Scholar], [Publisher]

[34] M. Arami, N.Y. Limace, N.M. Mahmoodi, N.S. Tabrizi, *J. Hazard. Mater. B,* **2006**, *135*, 171–179. [Crossref], [Google Scholar], [Publisher]

[35] J.O. Babalola, J.O. Olowoyo, A.O. Durojaiye, A.M. Olatunde, E.I. Unuabonah, M.O. Omorogie, *J. Taiwan. Inst. Chem. Eng.,* **2016**, *58*, 490–499. [Crossref], [Google Scholar], [Publisher]

[36] D. Kavitha, C. Namasivayam, *Dyes Pigments,* **2007**, *74*, 237–248. [Crossref], [Google Scholar], [Publisher]

[37] M. Anbia, Z. Parvin, *Chem. Eng. Res. Dev.*, **2011**, *89*, 641–647. [Crossref], [Google Scholar], [Publisher]

[38] A.A Adeyi, I.T. Popoola, A.S. Yusuff, A.S. Olateju, *J. Bioprocess. Chem. Eng.,* **2014**, *2*, 1–6. [Google Scholar], [Publisher]

[39] M.E. Argun, S. Dursun, C. Ozdemir, M. Karatas, *Journal of Hazardous Materials*, **2007,** *141*, 77–85. [Crossref], [Google Scholar], [Publisher]

[40] M.M. Ibrahim, *J. Environ. Chem. Eng.*, **2019**, *7*, 102848. [Crossref], [Google Scholar], [Publisher]

[41] X. Zhang, Y. Li, M. Li, H. Zheng, Q. Du, H. Li, Y. Wang, D. Wang, C. Wang, K., Sui, H. Li, Y. Xia, *J. Colloid Interface Sci.,* **2019**, *556*, 249-257. [Crossref], [Google Scholar], [Publisher]

[42] I. Langmuir, *Journal of America Chemical Society,* **1918**, *40*, 1361–1403. [Crossref], [Google Scholar], [Publisher]

[43] B. Royer, N.F. Cardoso, E.C. Lima, V.S.O. Ruiz, T.R. Macedo, C. Airoldi, *J.Colloid Interface Sci.*, **2009**, 336, 398-405. [Crossref], [Google Scholar], [Publisher]

[44] K. Vijayaraghavan, Y. Yun, *Biotechnology Advances*, **2008**, *26*, 266–291. [Crossref], [Google Scholar], [Publisher]

[45] J.O. Babalola, N.A.A. Babarinde, O.A. Popoola, V.O. Oninla, *The Pacific J. Sci. Tech.*, **2009**, *10*, 439-450. [Google Scholar], [Publisher]

[46] I.W. Tan, A.L. Ahmad, B.H. Hameed, *Desalination*, **2008**, *225*, 13-28. [Crossref], [Google Scholar], [Publisher]

[47] O.S. Bello, O.U. Bello, O.L. Ibrahim, *CJPL,* **2014**, *2*, 1–13. [Google Scholar], [Publisher]